Supporting Information

Unravelling the Origin of Operational Instability of Quantum Dot based Light-Emitting Diodes

Jun Hyuk Chang,[1] Philip Park,[2] Heeyoung Jung,[3] Byeong Guk Jeong,[4] Donghyo Hahm,[1] Gabriel Nagamine,[5] Jongkuk Ko,[6] Jinhan Cho,[6] Lazaro A. Padilha,[5] Doh C. Lee,[4] Changhee Lee,[3] Kookheon Char[1,] and Wan Ki Bae[7,*]*

[1]School of Chemical and Biological Engineering, Seoul National University, Seoul 08826, Korea

[2]Department of Chemistry and Biochemistry, University of California, Los Angeles, California 90095, USA

[3]School of Electrical and Computer Engineering, Inter-University Semiconductor Research Center, Seoul National University, Seoul 08826, Korea

[4]Department of Chemical and Biomolecular Engineering, KAIST Institute for the NanoCentury, Korea Advanced Institute of Science and Technology (KAIST), Daejeon 34141, Korea

[5]Instituto de Fisica "Gleb Wataghin", Universidade Estadual de Campinas, UNICAMP, P.O. Box 6165, 13083-859 Campinas, São Paulo, Brazil

[6]Department of Chemical and Biological Engineering, Korea University, Seoul 02841, Republic of Korea

[7]SKKU Advanced Institute of Nanotechnology (SAINT), Sungkyunkwan University, Suwon-si, Gyeonggi-do 16419, Korea

1. Characteristics of quantum dots (QDs) used in the present study

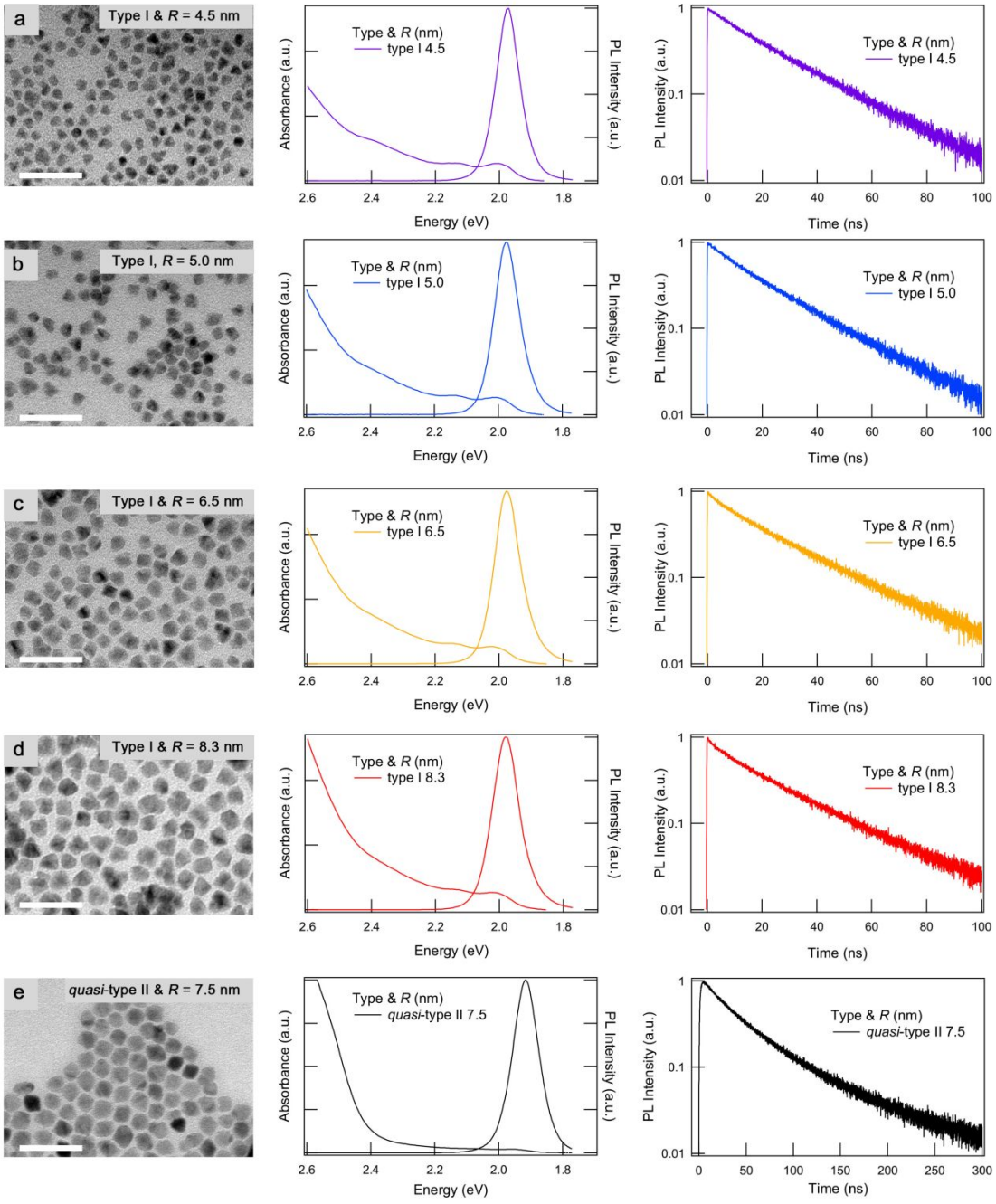

Figure S1. Characteristics of quantum dots used in the present study. TEM images (left) (scale bar, 50 nm), UV-vis and PL spectra (middle), and solution PL decay curves (right) of (a-d) CdSe(r = 2.0 nm)/$Cd_{0.5}Zn_{0.5}S$ QDs

(*h* = (a) 2.5, (b) 3.0, (c) 4.5, (d) 6.3 nm) type I QDs and (e) CdSe(*r* = 2.0 nm)/CdS(*h* = 5.5 nm) *quasi*-type II QDs.

Table S1. Structural and photophysical characteristics of type I QDs and quasi-type II QDs used in the present study.

QD notation	QD composition (core/shell)	Core radius (*r*, nm)/ shell thickness (*h*, nm)	Peak PL energy/ FWHM [eV/meV]	PL QY[a)] [%]	τ_x[b)] [ns]
type I 4.5	CdSe/$Cd_{0.5}Zn_{0.5}S$	2.0/2.5	1.97/86.8	81	21.5
type I 5.0	CdSe/$Cd_{0.5}Zn_{0.5}S$	2.0/3.0	1.97/92.9	80	20.1
type I 6.5	CdSe/$Cd_{0.5}Zn_{0.5}S$	2.0/4.5	1.97/95.4	81	20.5
type I 8.3	CdSe/$Cd_{0.5}Zn_{0.5}S$	2.0/6.3	1.98/98.7	80	20.1
quasi-type II 7.5	CdSe/CdS	2.0/5.5	1.92/96.2	67	45.3

a) PL QYs were measured using a spectrometer coupled with an integrating sphere (excitation wavelength: 520 nm); b) τ_x denotes the time when PL intensity becomes 1/e of initial PL intensity.

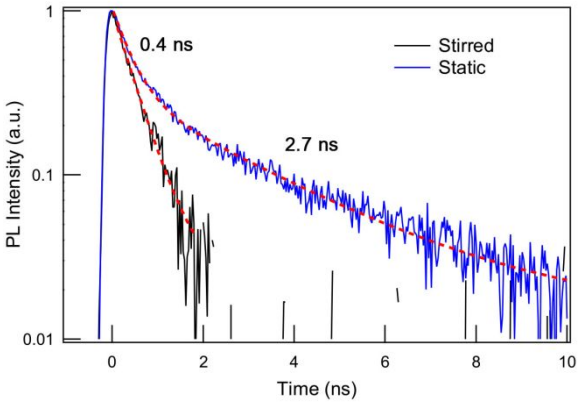

Figure S2. Negative trion (X^-) and biexciton (XX) lifetime in CdSe(r = 2.0 nm)/$Cd_{0.5}Zn_{0.5}S$(h = 6.3 nm) QDs. Extracted solution PL decay curves of CdSe(r = 2.0 nm)/$Cd_{0.5}Zn_{0.5}S$(h = 6.3 nm) QDs under static (blue) and stirred (black) conditions. PL decay curves are obtained by subtracting PL decay curves when average number of excitons per dot is 0.03 (<N> = 0.03) from that when average number of excitons per dot is 0.95 (<N> = 0.95). It is well-known that vigorous stirring during the measurements can decrease the ratio of trion on PL decay dynamics, by preventing slow accumulation of charged QDs in excitation volume.[1-3] By comparing PL decay dynamics of stirred and static conditions, we assessed biexciton (XX) and negative trion (X^-) lifetime of CdSe/$Cd_{0.5}Zn_{0.5}S$ QDs (τ_{XX} = 0.4 ns, τ_{X^-} = 2.7 ns). CdSe/$Cd_{0.5}Zn_{0.5}S$ QDs (R = 8.3nm) were excited at 520nm laser at a repetition rate of 200 kHz.

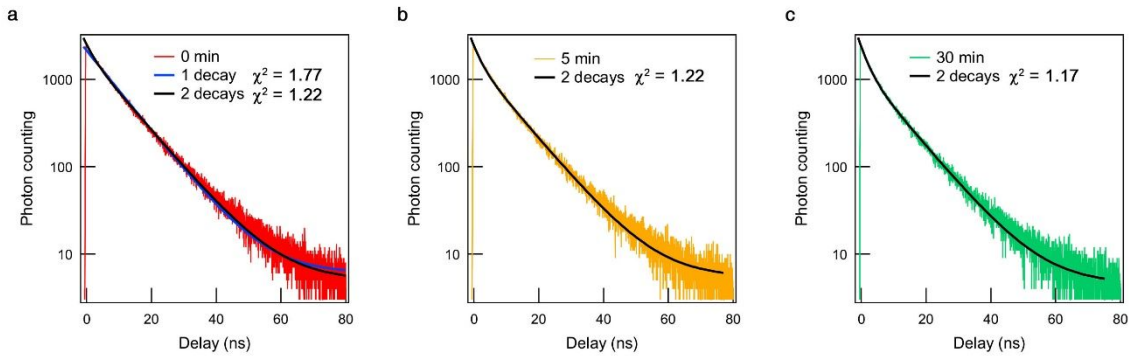

Figure S3. Goodness of fit with Chi-square. Figure 2c (PL decay dynamics of QD emissive layer within device after (a) 0, (b) 5, (c) 30 min of operation was fitted by (a) single-exponential and (a), (b), (c) bi-exponential equation. Chi-square is suggested at figure.

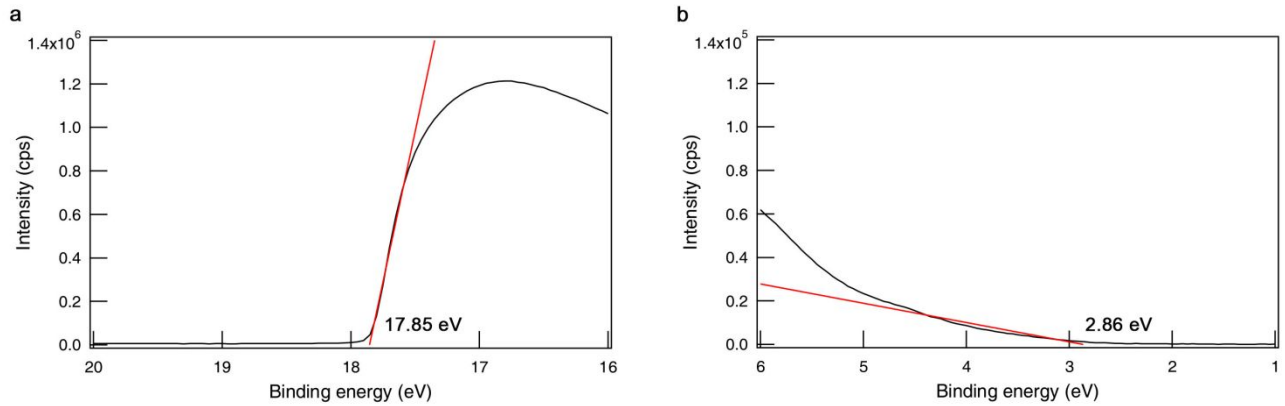

Figure S4. Lowest quantized electronic energy level of neutral CdSe(r = 2.0 nm)/$Cd_{0.5}Zn_{0.5}S$(h = 6.3 nm) QDs. Expanded UPS spectra of CdSe(r = 2.0 nm)/$Cd_{0.5}Zn_{0.5}S$(h = 6.3 nm) type I core/shell QDs at (a) high (16 - 20 eV) and (b) low binding energy regime (1 - 6 eV).

$1S_h$ energy level of CdSe(r = 2.0 nm)/$Cd_{0.5}Zn_{0.5}S$(h = 6.3 nm) QDs is estimated from UPS spectra as below.

$1S_h$ = 21.2 eV - |17.85 eV – 2.86 eV| = 6.21 eV

$1S_e$ energy level of QDs is then calculated by subtracting 1S energy obtained from absorption spectrum (Figure S1) from $1S_h$ energy as below.

$1S_e$ = 6.21 eV – 1.99 eV = 4.22 eV

2. Modeling of QD charging during QLED operation

The fraction of negatively charged QDs and the electron injection rate at a given time ($J_e(t)$) under constant current density (J_h = constant) can be obtained by considering coupled rate equations.

$$J_e(t) - J_h = \frac{dC(t)}{dt} \qquad \text{(eq. 1)}$$

$$J_e(t) = J_e(0)\left(1 - \alpha\frac{C(t)}{N}\right) \qquad \text{(eq. 2)}$$

where $J_e(t)$ and J_h is the number of injected electrons and holes into QDs in unit area (cm^2) at time t, N is the number of QDs in unit area (cm^2), $C(t)$ is the number of charged QDs in unit area (cm^2) at time t, and α is the repulsion coefficient for electron injection from ZnO ETL into negatively charged QDs.

From these equations, we can get the fraction of charged QDs and the electron injection rate at a given time ($J_e(t)$).

$$F(t) = C(t)/N = \frac{J_e(0) - J_h}{J_e(0)\ \alpha}\left(1 - \exp\left(-\frac{J_e(0)\alpha}{N}t\right)\right) \qquad \text{(eq. 1)}$$

$$J_e(t) = J_e(0) - (J_e(0) - J_h)\left(1 - \exp\left(-\frac{J_e(0)\alpha}{N}t\right)\right) \qquad \text{(eq. 2)}$$

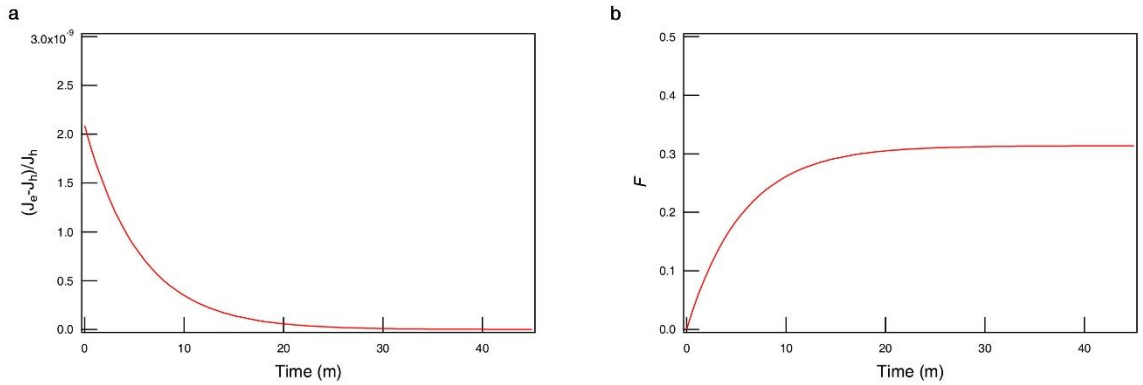

Figure S5. (a) The imbalance between electron and hole injection rate ($(J_e-J_h)/J_h$) and (b) the fraction of charged quantum dots (F) as a function of operation time.

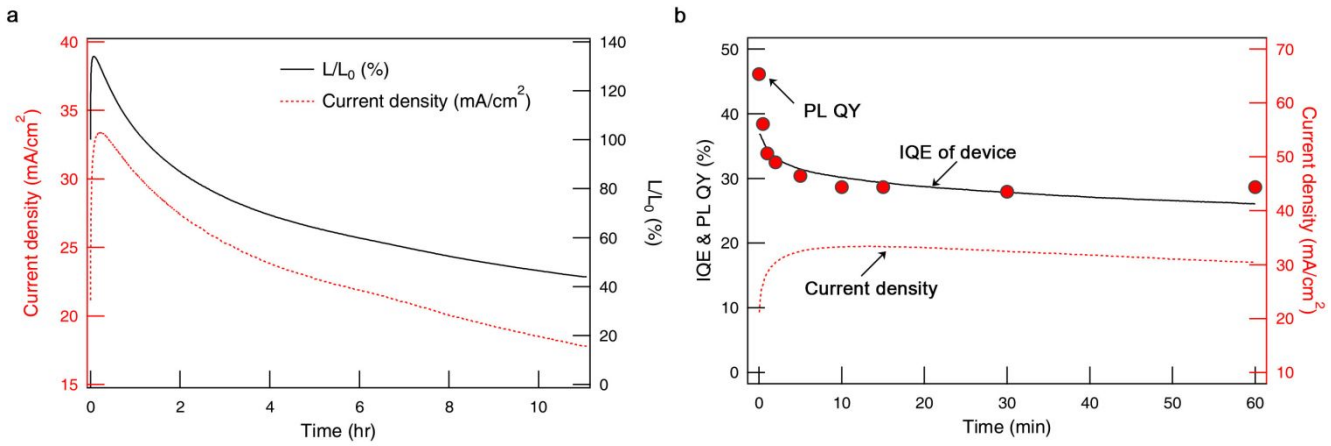

Figure S6. Time dependent device characteristics under constant operation voltage. (a) Operation time-dependent current density (red broken line) and relative brightness (black solid line) of QLED implementing CdSe(*r* = 2.0 nm)/$Cd_{0.5}Zn_{0.5}S$(*h* = 6.3 nm) QDs under the constant applied voltage (4V). (b) Operation time-dependent traces of IQE (black solid line) and the current density (red broken line) of QLED implementing CdSe(*r* = 2.0 nm)/$Cd_{0.5}Zn_{0.5}S$(*h* = 6.3 nm) QDs under the constant voltage (4V) and PL QYs (red circle) of the QD emissive film in the corresponding device. Current density increases substantially (1.58 times) in early operation regime (10 min) as a result of reduced hole injection barrier by the presence of excess electrons in the QD emissive layer.

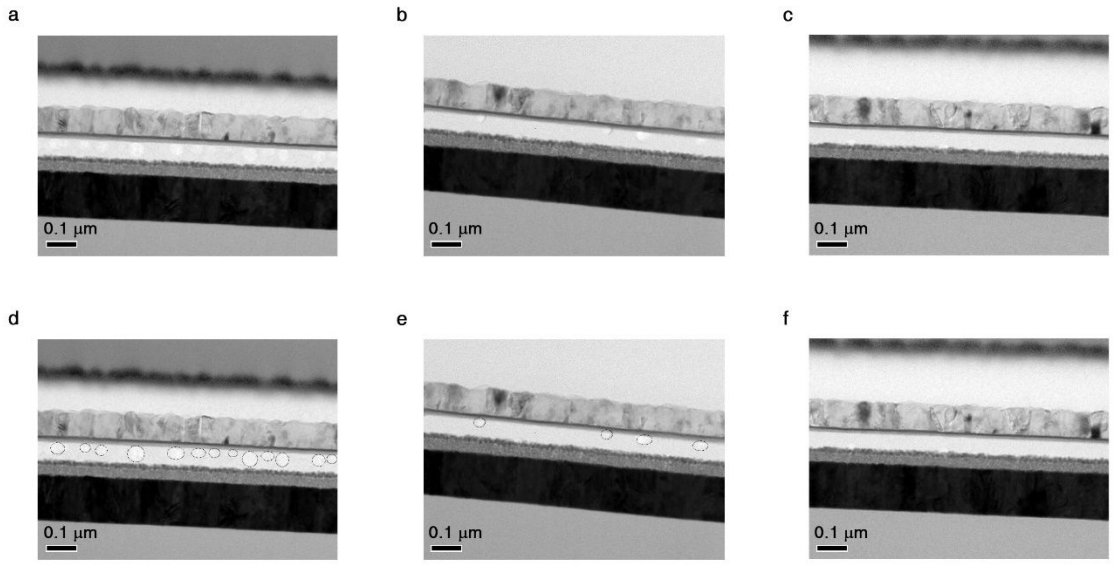

Figure S7. Cross-sectional TEM images of devices (a,d) as prepared, after (b,e) 45 hrs and (c,f) 90 hrs of operation at the applied current density of 30 mA/cm^2. The voids in CBP are marked in (d-f).

3. Calculation of lowest quantized electronic states of charged QDs

From neutral QD (QD^0) (Figure S5a), we performed a quantum mechanical calculation including self-consistency and dielectric mismatch effect in three dimensions to calculate energy level of CdSe(r = 2.0 nm)/$Cd_{0.5}Zn_{0.5}S$(h = 6.3 nm) QDs depending on their charging states (singly (QD^-), doubly negatively charged QDs (QD^{2-}) and singly positively charged QDs (QD^+)) (Figure S5b-d).

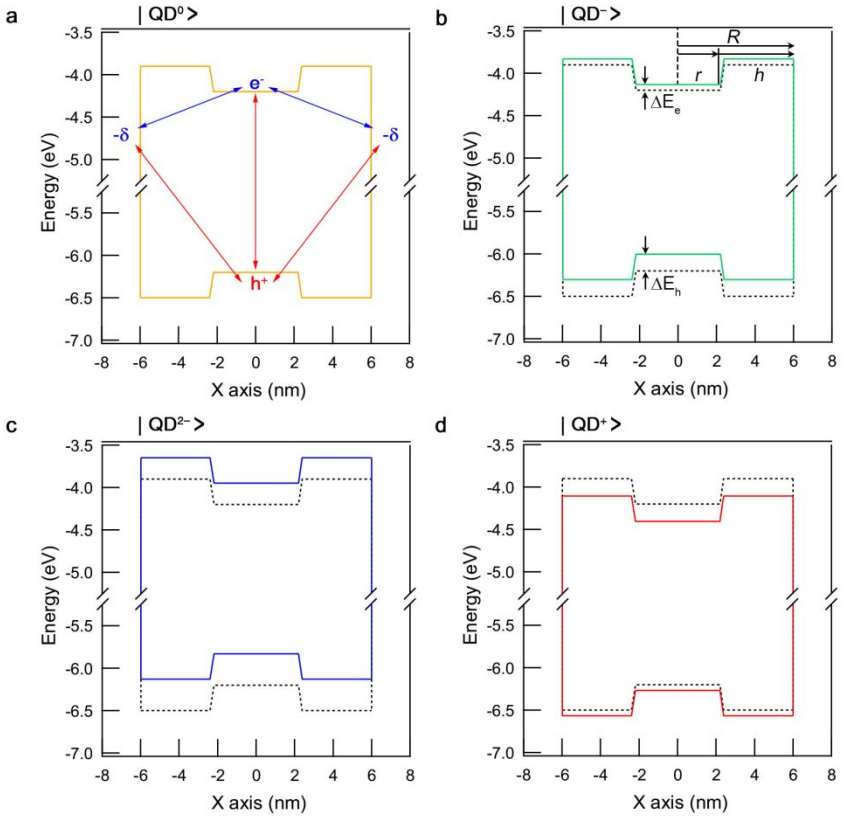

Figure S8. Simulation results of electron's and hole's band edge energy level of CdSe(r = 2.0 nm)/$Cd_{0.5}Zn_{0.5}S$(h = 6.3 nm) QD depending on their charging states. (a) neutral (QD^0), (b) singly (QD^-), (c) doubly negatively charged (QD^{2-}) and (d) singly positively charged QDs (QD^+).

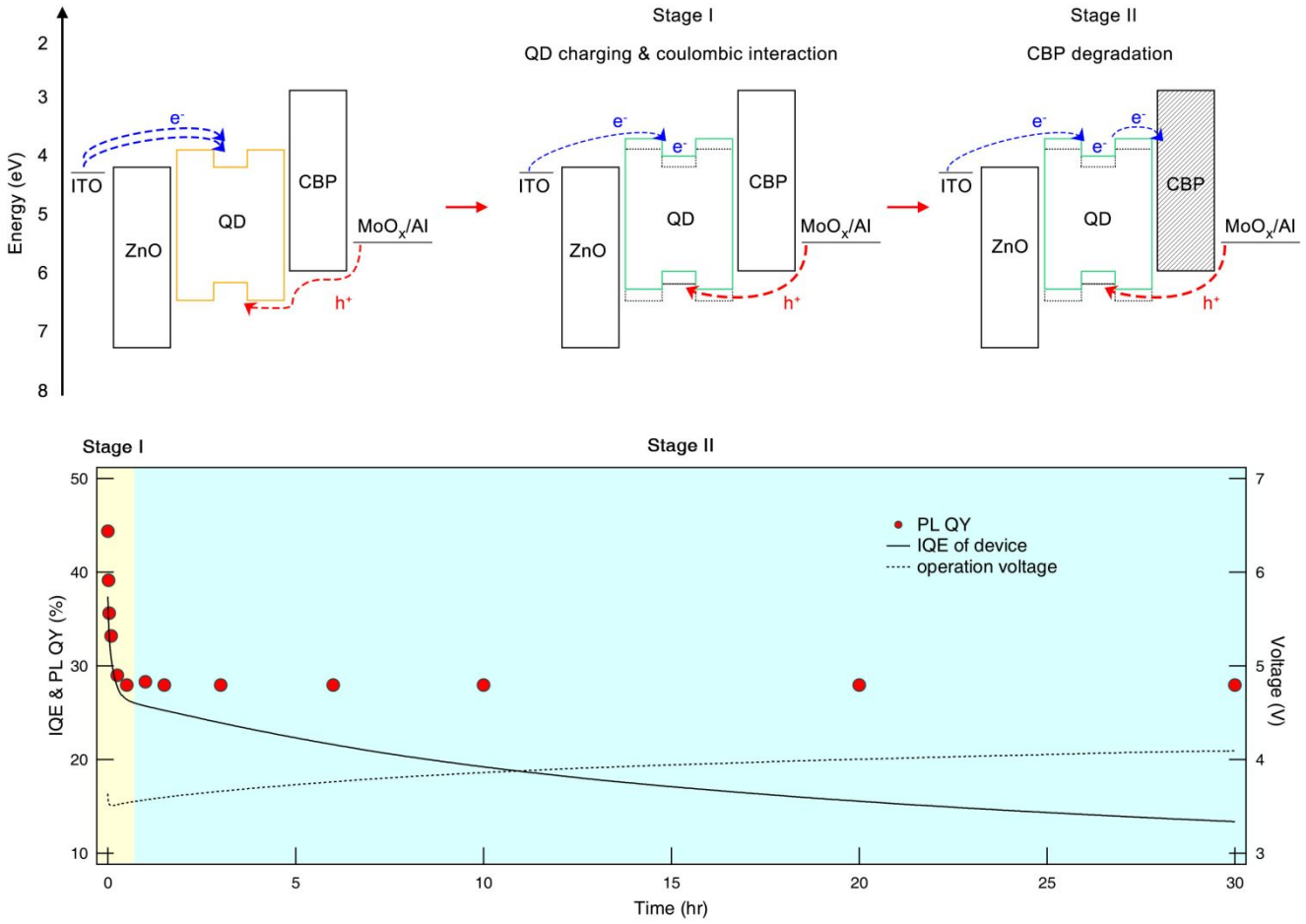

Figure S9. Sketches of the device degradation mechanisms in QLEDs under operation. The abrupt device efficiency loss during the early operation (Stage I) is as a result of the accumulation of excess electrons within the QD emissive layer that escalates the probability of non-radiative Auger recombination. The continuing reduction of the device efficiency after the change in the PL efficiency ceases (Stage II) originates from the mechanical damage in organic hole transport layer, which creates the non-radiative recombination centers within HTLs.

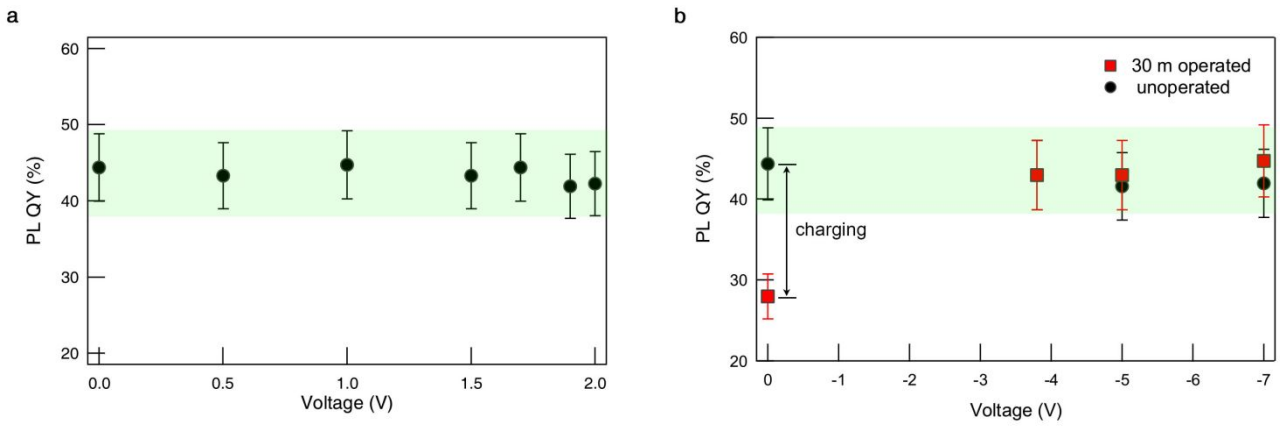

Figure S10. Applied voltage (*V*) dependent PL QY change of the QD emissive layer within the device. (a) PL QYs of CdSe/$Cd_{0.5}Zn_{0.5}S$ QD (*R* = 8.3nm) emissive film in QLED at the applied voltage below the turn-on voltage (2.2 V). We note that PL QY does not change before the turn-on voltage, indicating that spontaneous charging of QDs does not take place.[4] (b) PL QYs of the QD emissive film within unoperated (black circle) and 30 min operated (red square) QLEDs as a function of applied reverse voltage. QLEDs employing CdSe/$Cd_{0.5}Zn_{0.5}S$ QDs (*R* = 8.3nm) are tested.

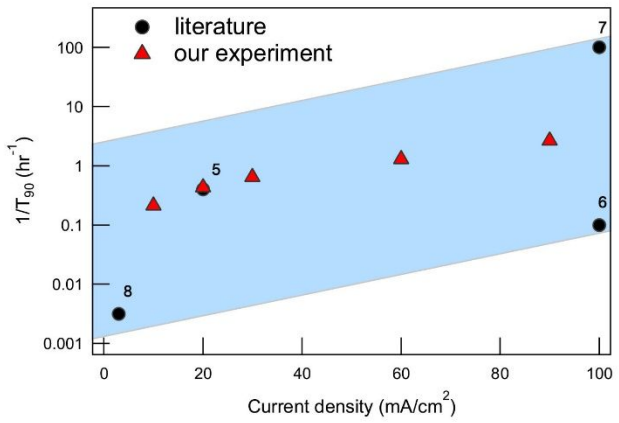

Figure S11. Overall degradation rate of QLEDs with similar efficiency under various current density.[5-8]

References

1. Bae, W. K.; Padilha, L. A.; Park, Y.-S.; McDaniel, H.; Robel, I.; Pietryga, J. M.; Klimov, V. I., Controlled Alloying of the Core–Shell Interface in Cdse/Cds Quantum Dots for Suppression of Auger Recombination. *ACS Nano* **2013**, *7*, 3411-3419.

2. Padilha, L. A.; Robel, I.; Lee, D. C.; Nagpal, P.; Pietryga, J. M.; Klimov, V. I., Spectral Dependence of Nanocrystal Photoionization Probability: The Role of Hot-Carrier Transfer. *ACS Nano* **2011**, *5*, 5045-5055.

3. McGuire, J. A.; Sykora, M.; Robel, I.; Padilha, L. A.; Joo, J.; Pietryga, J. M.; Klimov, V. I., Spectroscopic Signatures of Photocharging Due to Hot-Carrier Transfer in Solutions of Semiconductor Nanocrystals under Low-Intensity Ultraviolet Excitation. *ACS Nano* **2010**, *4*, 6087-6097.

4. Bae, W. K.; Park, Y.-S.; Lim, J.; Lee, D.; Padilha, L. A.; McDaniel, H.; Robel, I.; Lee, C.; Pietryga, J. M.; Klimov, V. I., Controlling the Influence of Auger Recombination on the Performance of Quantum-Dot Light-Emitting Diodes. *Nat. Commun.* **2013**, *4*, 2661.

5. Kwak, J.; Bae, W. K.; Lee, D.; Park, I.; Lim, J.; Park, M.; Cho, H.; Woo, H.; Yoon, D. Y.; Char, K., Bright and Efficient Full-Color Colloidal Quantum Dot Light-Emitting Diodes Using an Inverted Device Structure. *Nano Lett.* **2012**, *12*, 2362-2366.

6. Dai, X.; Zhang, Z.; Jin, Y.; Niu, Y.; Cao, H.; Liang, X.; Chen, L.; Wang, J.; Peng, X., Solution-Processed, High-Performance Light-Emitting Diodes Based on Quantum Dots. *Nature* **2014**, *515*, 96-99.

7. Mashford, B. S.; Stevenson, M.; Popovic, Z.; Hamilton, C.; Zhou, Z.; Breen, C.; Steckel, J.; Bulovic, V.; Bawendi, M.; Coe-Sullivan, S., High-Efficiency Quantum-Dot Light-Emitting Devices with Enhanced Charge Injection. *Nat. Photon.* **2013**, 7, 407-412.

8. Yang, Y.; Zheng, Y.; Cao, W.; Titov, A.; Hyvonen, J.; Manders, J. R.; Xue, J.; Holloway, P. H.; Qian, L., High-Efficiency Light-Emitting Devices Based on Quantum Dots with Tailored Nanostructures. *Nat. Photon.* **2015**, *9*, 259-266.